Official English translation https://doi.org/10.18500/0869-6632-2019-27-3-9-32

The effect of parametric processes on the propagation of spin waves in cross-shaped structures based on waveguides from yttrium iron garnet films

A. V. Kozhevnikov[1], *Y. V. Khivintsev*[1,2], *V. K. Sakharov*[1], *G. M. Dudko*[1], *S. L. Vysotskii*[1,2], *Y. V. Nikulin*[1,2], *E. S. Pavlov*[1], *Y. A. Filimonov*[1,2], *A. G. Khitun*[3]

[1]Kotel'nikov Institute of Radio Engineering and Electronics, Saratov branch, Russian Academy of Sciences, 38 Zelenaya, Saratov, Russia, 410019
[2]Chernyshevsky Saratov State University, 83 Astrakhanskaya str., Saratov, Russia, 410012
[3]Department of Electrical and Computer Engineering, University of California-Riverside, 900 University Ave., WCH 414, Riverside, CA, USA, 90815
E-mail: kzhavl@gmail.com, khivintsev@gmail.com, valentin@sakharov.info, dugal_2010@hotmail.com, vysotsl@gmail.com, yvnikulin@gmail.com, gekapavlov@gmail.com, yuri.a.filimonov@gmail.com, akhitun@engr.ucr.edu
Correspondence should be addressed to Kozhevnikov Alexander Vladimirovich, kzhavl@gmail.com
Received 14.12.2018, accepted for publication 22.03.2019

Topic. In this work, we experimentally explore the spin waves (SW) propagation in tangentially magnetized cross-like structure in the shape of two orthogonal waveguides on the base of yttrium iron garnet (YIG) film for the conditions when the first order parametric processes take place. **Aim.** We studied the influence of parametric processes on spectrum of SW in the tangentially magnetized cross-like structure in the filtration band defined as the frequency interval $\Delta f^{\parallel,\perp}$ of the overlapping spectra of SWs in longitudinally and transversely magnetized waveguides. **Methods.** The experiments were carried out with the cross-like structure from YIG film with the thickness $d \approx 3.8$ μm, having the form of two orthogonal waveguides with the width $w \approx 500$ μm, length $L \approx 3$ mm, and wire SW antennas placed at the ends of waveguides. One of the antennas was considered as the input and was used to excite SW in the structure, and the other three were used to analyze the spectrum of output signals with the frequencies inside the filtration band $\Delta f^{\parallel,\perp}$. **Results.** It was shown that the shape of SW spectrum obtained at the output antennas of orthogonal waveguides could be significantly changed when the SW parametric instability takes place. **Discussion.** We attribute this effect to the formation of secondary SW-satellites in the spectrum of the pump signal and the influence of lateral quantization effects on SW spectrum in the studied cross-like structure.

Key words: parametric spin waves, spin wave interference, microwave guide, spintronics, magnonics, micromagnetic modeling.

Reference: Kozhevnikov A.V., Khivintsev Y.V., Sakharov V.K., Dudko G.M., Vysotskii S.L., Nikulin Y.V., Pavlov E.S., Filimonov Y.A., Khitun A.G. The effect of parametric processes on the propagation of spin waves in cross-shaped structures based on waveguides from yttrium iron garnet films. *Izvestiya VUZ, Applied Nonlinear Dynamics*, 2019, vol. 27, no. 3, pp. 9–32. https://doi.org/10.18500/0869-6632-2019-27-3-9-32

Acknowledgements. The study was carried out with the financial support of the Russian Science Foundation (project № 17-19-01673)

Introduction

One of the significant drawbacks of the electronic element base of information systems based on CMOS technologies is the rapid increase in Joule losses associated with charge transfer as the number of transistors and interstitial connections in microprocessors increases. An approach based on using the direction of the electron spin [1–3] is considered as one of the alternatives allowing one to abandon the use of an electron charge as a logical "0" or "1".

The use of spin current (not related to charge transfer) opens up a wide range of possibilities to create energy-efficient information processing technologies on the principles of spintronics and magnonics, where the spin waves (SW) are utilized as a source for the spin current and as an information carrier [4–5]. Such technologies can be based on effects of constructive and destructive interference of SW during propagation in magnonic networks, in particular, based on a system of orthogonal waveguides [6–9]. For this reason, the features of the propagation of SW in cross-shaped structures from orthogonal waveguides recently received considerable attention [9–18]. It was shown that in nodes of the magnetized cross-shaped structure, the effective transmission of the SW signal to the orthogonal channel is carried out in a certain frequency band $\Delta f^{\parallel,\perp}$, in order of magnitude coinciding with the frequency difference of the long-wavelength boundaries of the spectra of longitudinally ($f_0^{\parallel}$) and transversely ($f_0^{\perp}$) magnetized waveguides ($\Delta f^{\parallel,\perp} \approx \Delta f_0^{\parallel,\perp} = f_0^{\parallel} - f_0^{\perp}$). Thanks to such filtering properties, the magnetic cross with four SW antennas located at the ends will act as a Mach–Zehnder type interferometer at frequencies $f \in \Delta f^{\parallel,\perp}$. In this case, the effects of microwave interference in magnetic crosses can be used to create magnonic holographic memory [19], reversible logic [20], database processing technologies [21], magnetic field sensors [22], and to determine the properties of magnetic microparticles [23].

Note that in most experiments, the propagation of SW in crosses based on films of yttrium iron garnet (YIG) and at power levels of input signals P_{in} below threshold values P_{th} for the development of parametric instability ($P_{in} < P_{th}$) was studied. Meanwhile, it is well known [24–31] that, in YIG films, which are characterized by the lowest relaxation rate for SW the threshold of parametric instability of the first order does not usually exceed $P_{in} \approx 1...10$ mW, which is easily realized experimentally. It is essential that for the development of parametric instability, in addition to the condition $P_{in} > P_{th}$, the pump frequency f_p and the magnetization field H must be chosen in such way that the conservation laws are satisfied [24]

$$f_p = f_1 + f_2, \tag{1}$$

$$\vec{k}_p = \vec{k}_1 + \vec{k}_2. \tag{2}$$

In conservation laws (1), (2), the frequencies $f_{p,1,2}$ and the wave vectors $\vec{k}_{p,1,2}$ correspond to pumping and parametric spin waves. The development of such parametric instability leads to a limitation of the power of the SW signal at the pump frequency and to the appearance of satellite-frequencies in the output signal spectrum [27, 28]. Both of these processes can influence the result of interference of waves in the cross. On the other hand, the influence of parametric instability on the propagation of SW in cross-like structures may differ from the cases of film structures considered earlier [27–31]. Indeed, the presence of filtering properties in cross-shaped structures, on the one hand, as well as the presence of a pair of output antennas oriented orthogonally to the input transducer, on the other hand, can lead to qualitative differences in the spectra of output signals. It should be added that in cross-shaped structures made of waveguides of finite width w, the propagation of SW can be

affected by the lateral quantization of the SW spectrum [32], which can also affect the conditions for the formation of satellite waves in the spectrum. In addition, it should be noted that nonlinear spin-wave effects in planar magnonic structures were also studied in [33, 34]. The features of the transformation of surface SW into backward volume SW in curved magnetic waveguiding structures were considered in [35].

The aim of this work was an experimental study of the influence of the development of the first order parametric instability on the propagation of SW in cross-like structures based on a YIG film.

1. The investigated structure and experimental results

The propagation of SW in the cross-like structure shown in Fig. 1. was studied. 1. The cross was formed by laser ablation from a YIG film with a thickness $d \approx 3.8$ μm grown by liquid-phase epitaxy on a substrate of gadolinium-gallium garnet with a thickness of 500 μm. The film had an effective saturation magnetization $4\pi M_0 \approx 1876$ G and a ferromagnetic resonance (FMR) linewidth $\Delta H \approx 0.5$ Oe. The waveguides had a width $w \approx 500$ μm and a length $L \approx 3$ mm (see the inset in Fig. 1). The structure was located on a non-magnetic metal base, where coaxial junctions were also built-up, connected to four SW antennas in the form of a gold wire with a diameter of 30 μm and a length of about 0.6 mm, located at a distance of $100...200$ μm from the edges of the waveguides. Antenna 1 was used to excite SW, and the remaining antennas 2, 3, 4 were as receiving ones. The sample was placed in the gap between the poles of the electromagnet so that the magnetic field H was directed in the plane of the structure and oriented either parallel (Fig. 2, *a*) or perpendicularly (Fig. 2, *b*) to input transducer 1.

Fig. 2 shows a block diagram of an experimental setup. The input signal from the network analyzer 1 ENA Agilent E5071C through the power amplifier 3 “Mikran” MAHW010120 and adjustable attenuator 5 was fed to port 1 of the structure. In this case, the maximum level of incident power was $P_{in} \approx 100$ mW in the frequency range of 1...8 GHz. The output signals from ports 2, 3, 4 of the studied structure through the microwave switch and microwave broadband amplifier 4 Agilent Technologies Preamplifier 87405C were fed to an Agilent N9320A spectrum analyzer 2.

While investigating the influence of parametric processes on the propagation of SW in the YIG structure under considiration, an approach, typical for the study of nonlinear SW in films, was used [24–31]. The influence of the power of the input signal P_{in} on the form of the spectrum of the output signal at a fixed frequency f_p was considered, as well as the frequency dependence of the transmission parameters $S_{ij}(f) = 10\log(P_i^{out}/P_j^{in})$ between ports with number j, where the input signal was received, and with number i, from where the output signal with the power P_{out} was taken. It was taken into account that conservation laws (1), (2), the fulfillment of which is necessary for the development of the first order parametric instability (three-magnon), are allowed only in the range of frequencies and bias fields, where condition [27] is satisfied

$$f_p \geq 2f_{min}. \tag{3}$$

Here f_{min} is the minimum frequency (bottom frequency) in the SW spectrum, which, neglecting the influence of inhomogeneous exchange and anisotropy fields, coincides with the short-wavelength ($k \to \infty$) boundary of the spectrum of backward volume spin waves (BVSW) traveling along the field direction $\vec{H}$ [24, 25], the frequency $f_H = \gamma H$, where $\gamma = 2.8$ MHz/Oe is the gyromagnetic ratio in the YIG. Note that the effect of inhomogeneous exchange on the position of the “bottom” of the SW

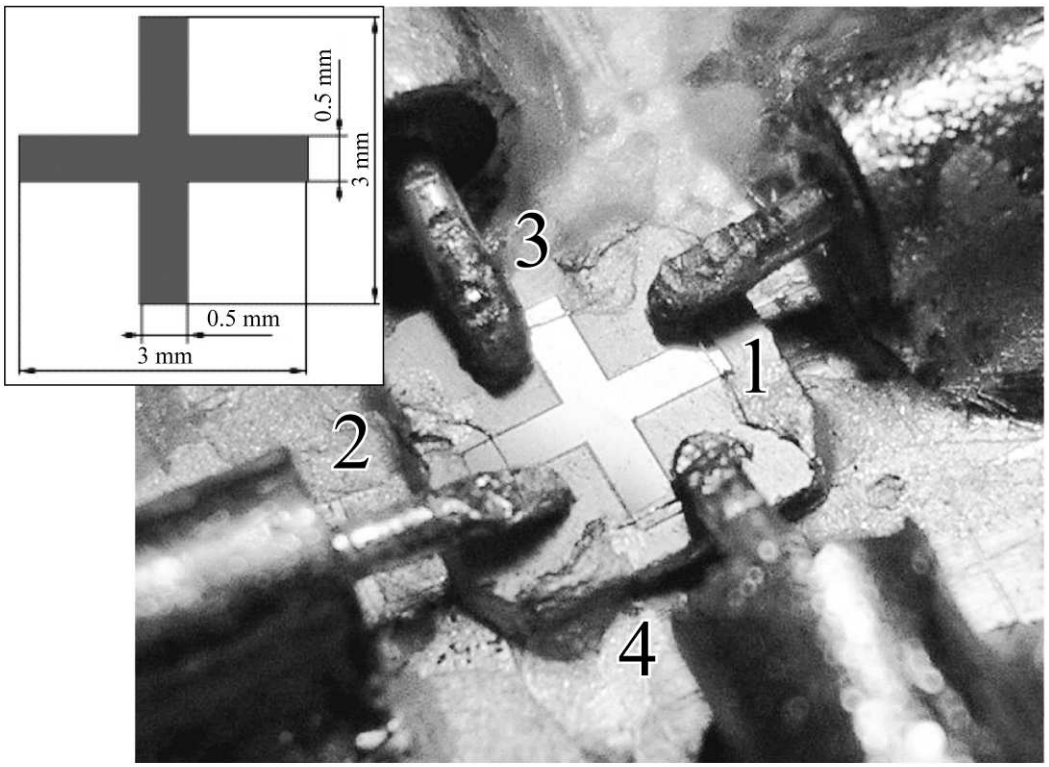

Fig. 1. View of the studied structure and experimental wiring. Inset shows the planar dimensions of the structure. Numbers 1,...,4 denote the gold wire antennas with the diameter of 30 μm and length of 0.6 mm, spaced by 100...200 μm from the sample edges

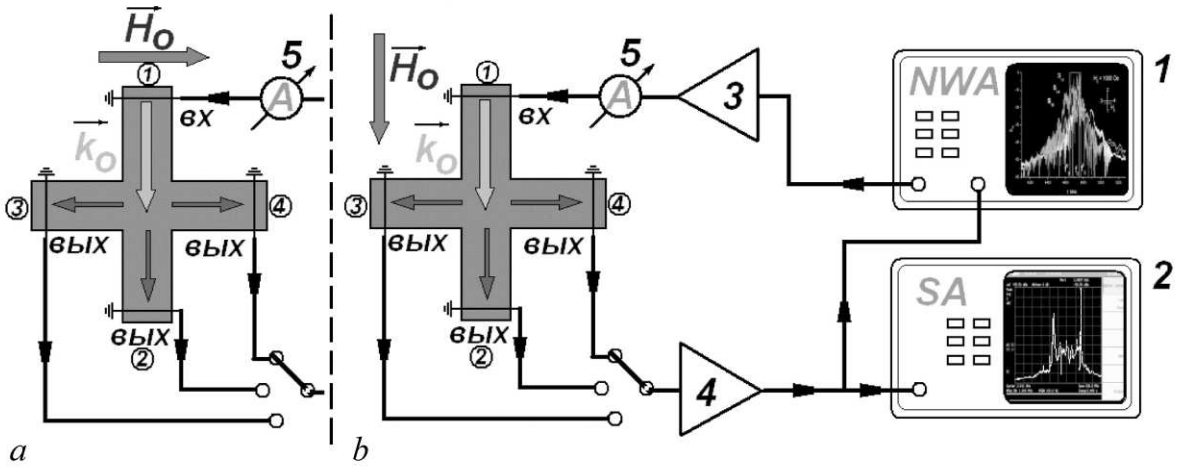

Fig. 2. Block diagram of the experimental setup: *1* – vector network analyzer Agilent ENA E5071C; *2* – Agilent N9320A spectrum analyzer; *3* – power amplifier «Mikran» MAHW010120; *4* – wideband amplifier Agilent Technologies Preamplifier 87405C; *5* – attenuator. Figure fragments *a* and *b* correspond to the position of studied sample between the poles of electromagnet, so that the field produced by the electromagnet is parallel and perpendicular to antenna 1, respectively

spectrum begins to noticeably affect films with thickness $d \leq 1$ μm [36]. For the structure considered here based on a YIG film with a thickness $d \approx 3.8$ μm, the "exchange" shift of the "bottom" to the high-frequency region will be approximately 90 MHz [30] (see Fig. 7 below).

Below, we will consider the results obtained at pump frequencies $f_{p1} \approx 3$ GHz and $f_{p2} \approx 2.7$ GHz. In this case, the interval of the bias fields was chosen to take into account the need to fulfill the condition (3) and was in the range $390 \leq H \leq 510$ Oe.

Figure 3 shows the transmission spectra Si1(f) of the structure for the bias field $H = 470$ Oe when using antenna 1 as input and antennas with numbers $i = 2, 3, 4$ as output. Fig. 3, *a*, *b*, *c*, *d* correspond to the orientation of the magnetic field parallel and perpendicular to antenna 1 (see also Fig. 2). Dependences $S_{i1}(f)$ in Fig. 3, *a*, c were obtained at the input power level P_{in} below the threshold P_{th} for the development of parametric instability $P_{in} < P_{th}$, while the results presented in Fig. 3, *b*, *d*, reflect the case of $P_{in} > P_{th}$.

In the linear mode, the shape of the transmission spectra $S_{i1}(f)$ is consistent with the results of [11], where a cross with similar parameters was studied. From the shape of the transmission spectra $S_{31,41}(f)$ shown in Fig. 3, *a*, *c*, we can conclude that there are filtering properties for the structure under consideration. If we take the frequency range limited by the level of -20 dB from the level of minimum losses in the characteristics $S_{31,41}(f)$ as the "working" band $\Delta\Omega$, then the "working" filtering band will be $\Delta\Omega^{\perp} \approx 0.18$ GHz for Fig. 3, *a* and $\Delta\Omega^{\parallel} \approx 0.31$ GHz for Fig. 3, *p*.

For $P_{in} > P_{th}$, the values $S_{i1}(f)$ decrease significantly (see Fig. 3, *b*, *d*). Such behavior under the conditions of the development of three-magnon decays is well known [24–26] and reflects the nonlinear character of the $P_{out}(P_{in})$ dependence due to the limitation of the SW amplitude beyond the threshold of development of the instability of the pump wave with respect to three-magnon decays. For this reason, the amplitude of the characteristics $S_{i1}(f)$ in Fig. 3, *b*, *d* noticeably decreases at those frequencies where the processes (1), (2) for the excited SW are allowed. Moreover, this decrease occurs non-uniformly in the frequency range, which is explained by the non-uniformity of the nonlinear losses introduced by the three-magnon processes in the analyzed frequency band. Therefore, it is not possible to use the approach proposed for the case of $P_{in} < P_{th}$ to determine the cross filtration band $\Delta\Omega$ in the case of $P_{in} > P_{th}$. In this case, the degree of influence of parametric processes on the filtering properties of the structure in the region of intersection of waveguides, which determines the "working" frequency band $\Delta\Omega$, remains unclear.

To answer this question, we measured the parameters $S_{31}(f)$ and $S_{41}(f)$ in the linear mode ($P_{in} < P_{th}$), but in the presence on the antenna 2 of the pump signal P_p at a frequency $f_p \approx 3$ GHz with power $P_p > P_{th}$. It turned out that their characteristics are close to the linear case shown in Fig. 3, *a*, *c* (see curves 3 and 4 in Fig. 3, *e*, *f*). At the same time, pumping from antenna 2 did not affect the width of the "working" frequency band. Therefore, at the used incident power levels $P_{in} \approx 100$ mW, the dimensions of the nonequilibrium portion of the film, where the magnon density differs markedly from the equilibrium, do not capture the region of intersection of the waveguides.

Figures 4–6 show the spectra of the pump signal at the output antennas 2, 3, 4, depending on the magnitude H of the bias field and at different above-critical values of pumping $C = 10\log(P_{in}/P_{th})$. For Fig. 4 and 5, the magnetic field is directed parallel to the input transducer 1. The spectra shown in Fig. 6 are obtained when the sample was oriented in the electromagnet gap in such a way that the field H was perpendicular to antenna 1. From the figures 4–6 one can see that under conditions of the development of three-magnon decays, the spectra of the output SW signals at different ports of the studied cross-shaped structure can noticeably differ. Let us consider the possible mechanisms of this behavior of the spectra of output signals.

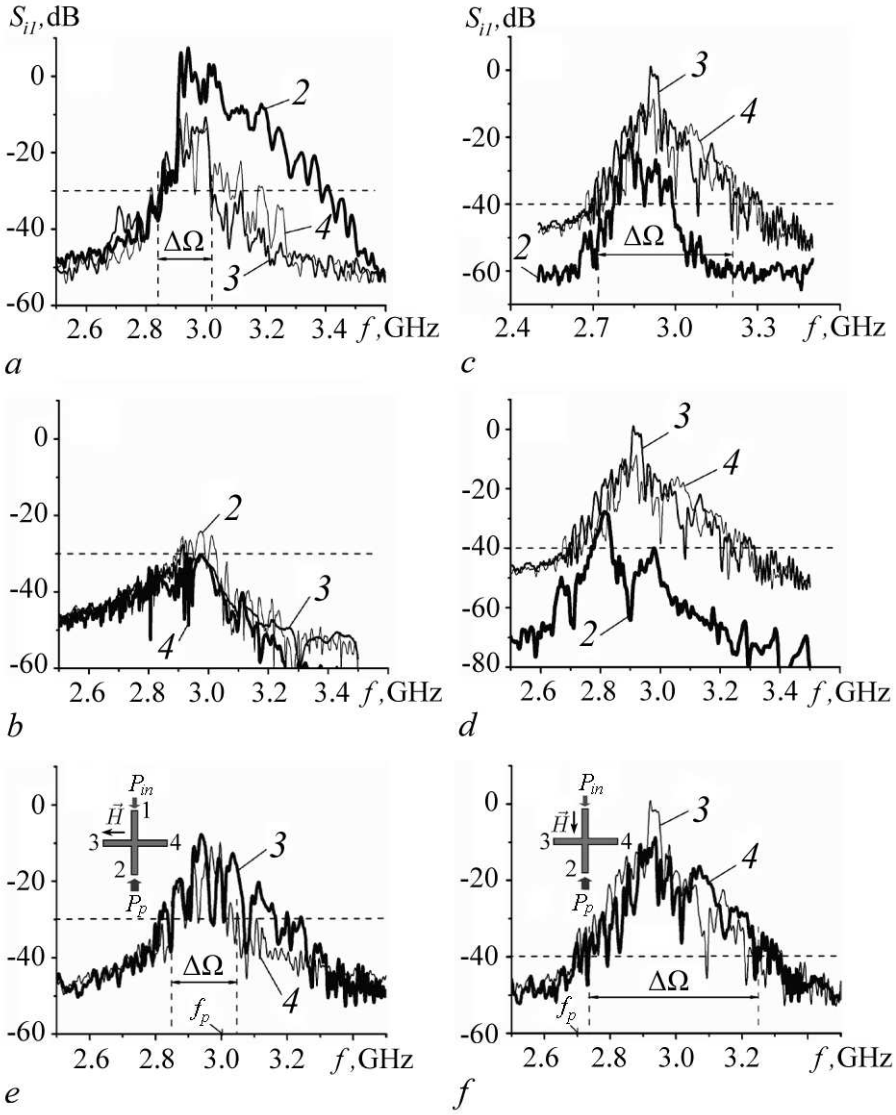

Fig. 3. *a*, *c* – SW transmission spectra in the structure at the input power level P below the threshold P_{th} for parametric instability launching $P < P_{th}$; *b*, *d* – just the same for the case when $P > P_{th}$. Fragments *a*, *b* correspond to the field $\vec{H}$ direction when it is parallel to the transducer 1 (see Fig. 2, *a*); fragments *c*, *d* correspond to the field $\vec{H}$ direction as shown in Fig. 2, *b*; in fragments *e*, *f* the arrow on the frequency axis shows the position of the pump frequency f_p for the corresponding magnetization geometries; f_p is the frequency at which the dependencies of the spectrum on the input power level were studied. The numbers *2*, *3*, *4* in the figures denote the transmission spectrum $S_{i1}(f)$ from the output antennas 2, 3 and 4, which locations are shown in Fig. 1, 2

2. Discussion of the experimental results

First of all, we obtain the estimated expressions for the filtering band $\Delta\Omega$ of the structure, determined from the experimental results in Fig. 3. For this, we consider the SW propagation mechanism in cross-shaped structures and take into account that the SW spectrum is essentially determined by the orientation of the SW wave vector $\vec{k}$ with respect to the magnetic field $\vec{H}$ [24, 25]. For the bias field direction shown in Fig. 2, *a* and *b*, the input transducer 1 excites respectively, surface (SSW) and backward volume (BVSW) spin waves. In infinite uniformly magnetized films, the SSW and BVSW spectra occupy non-overlapping frequency ranges $[f_s, f_0]$ and $[f_0, f_H]$, where $f_0 = \sqrt{f_H^2 + f_H f_m}$, $f_m = \gamma 4\pi M_0$, $f_s = f_H + 0.5 f_m$. In cross-shaped structures based on waveguides of width w due to demagnetization fields and lateral quantization along the width w, overlapping of the SSW and BVSW spectra is possible. Indeed, if the sections of the structure on which the SW antennas are located are considered as uniformly magnetized ellipsoids, then, for them, the frequency of uniform ferromagnetic resonance can be represented as [24]

$$f_0 = \sqrt{[f_H + (N_{11} - N_{33}) f_m][f_H + (N_{22} - N_{33}) f_m]}, \tag{4}$$

where N_{ii} are the components of the demagnetization tensor of the anisotropy of the form $\sum_i N_{ii} = 1$. It is believed that magnetization and the external field are directed along the $\vec{e}_3$ axis. If we further assume that the relation $L \gg w \gg d$ is fulfilled for the length L, width w, and thickness d of the waveguide, then the main contribution to (4) will be the demagnetization coefficients along the thickness N_d and the waveguide width N_w ($N_d \gg N_w$, $N_d \approx 1 - N_w$) Then, for a longitudinally magnetized waveguide, expression (4) takes the form

$$f_0^{\parallel} = \sqrt{[f_H + (1 - N_w) f_m][f_H + N_w f_m]} = \sqrt{f_0^2 + N_w (1 - N_w) f_H f_m}, \tag{5}$$

and for a transversely magnetized waveguide

$$f_0^{\perp} = \sqrt{[f_H + (1 - 2N_w) f_m][f_H - N_w f_m]} = \sqrt{f_0^2 - N_w f_m (3 f_H + 2 N_w f_m + f_m)}. \tag{6}$$

Therefore, the overlap of the SSW and BVSW spectra will be in the frequency interval $\Delta f_0^{\parallel,\perp} = f_0^{\parallel} - f_0^{\perp}$, defined as

$$\Delta f_0^{\parallel,\perp} \approx \frac{2 N_w f_m (f_H + 0.25 f_m)}{f_0}. \tag{7}$$

For a cross with selected parameters and with the magnitude of the components of the demagnetization tensor along the waveguide width $N_w \approx 0.015$ calculated using the formulas of [37], expression (7) gives the value $\Delta f_0^{\parallel,\perp} \approx 0.14$ GHz.

The effects of spectrum quantization along the width of the waveguide will lead to the appearance of "width" SSW and BVSW modes supported by waveguides. Such "width" modes are characterized by a continuous series of values of the projections of the longitudinal component $k_{\parallel}$ of the wave vector $\vec{k}$ onto the axis of the waveguide, and a discrete set of values of the projections $k_{\perp}$ into the direction perpendicular to the axis of the waveguide. The transverse component in the approximation of uniformity of the ground state of the waveguide takes values [32]

$$k_{\perp} = \frac{\pi n}{w}, \tag{8}$$

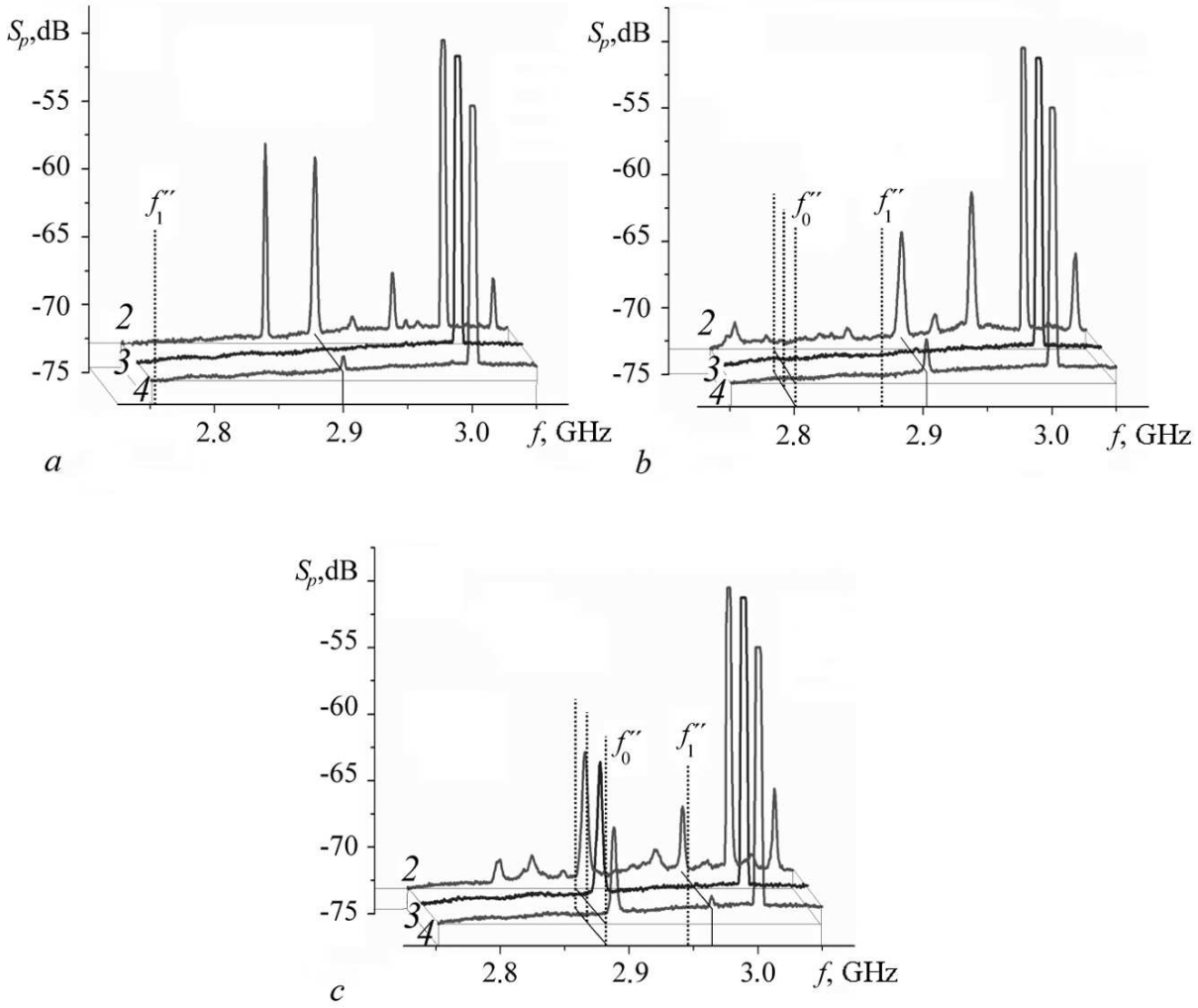

Fig. 4. View of the signal spectrum at the output antennas 2, 3 and 4 at the pump frequency of 3.0 GHz and magnetic field of: *a* – 400 Oe, *b* – 430 Oe, *c* – 450 Oe. The numbers at the curves correspond to the antenna number. The magnetic field $\vec{H}$ is parallel to the input antenna 1 (see Fig. 2, *a*). Above-critical value of pumping is $\approx 21...29$ dB. The dotted lines show the positions of the frequency $f_0^{\parallel}$ corresponding to the uniform ferromagnetic resonance in the longitudinally magnetized waveguide that is 3 mm long, 0.5 mm wide, 4 μm thick, and the frequency $f_1^{\parallel}$ of the first width mode in this waveguide

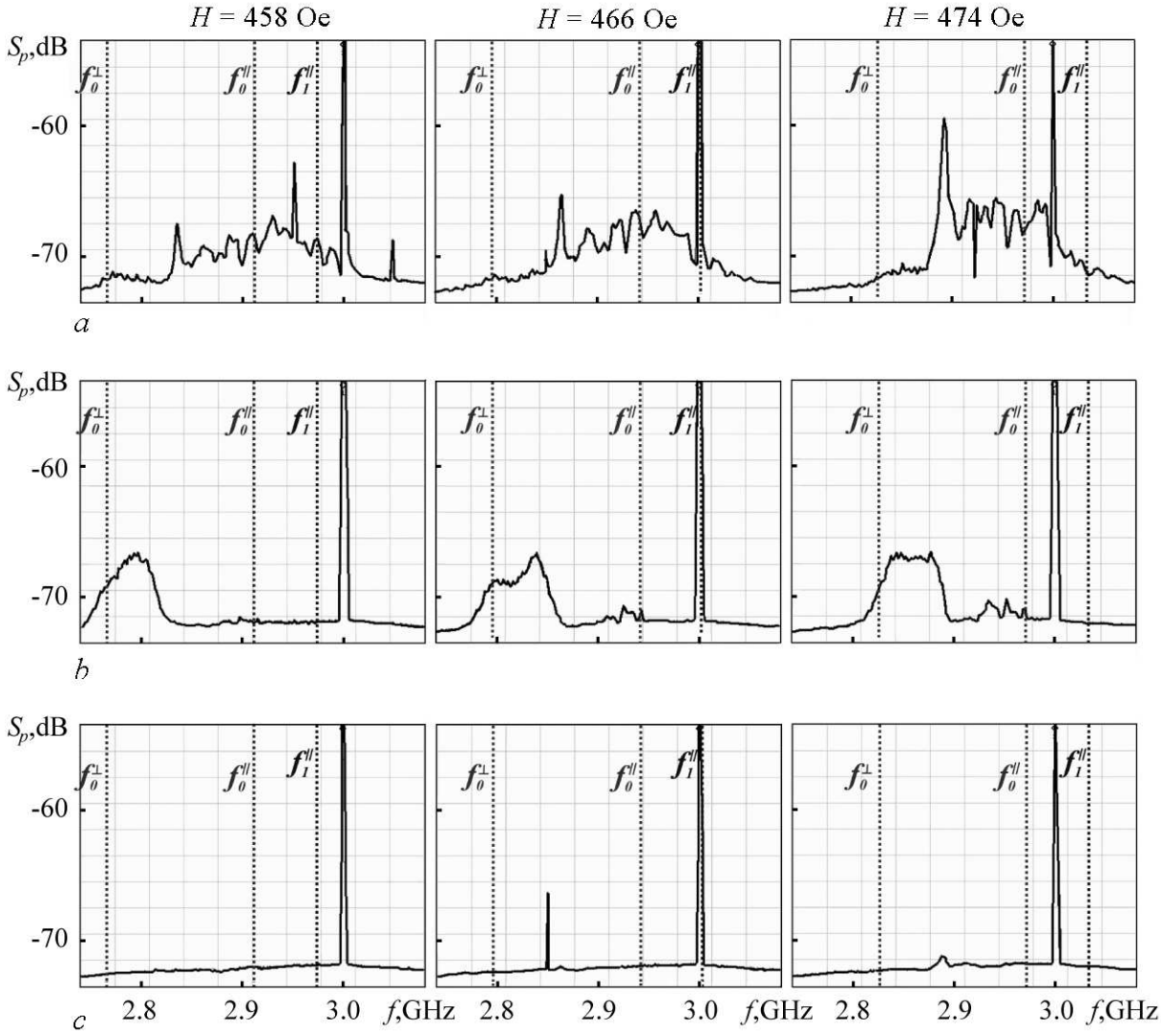

Fig. 5. The signal spectrum measured at the frequency of pumping at the output antennas: *a* – 2, *b* – 3, *c* – 4 with above-critical value of pumping $\approx$ 31...38 dB, depending on the magnitude of the magnetic field. The magnetic field values are shown in the figures. The direction of the magnetic field $\vec{H}$ is parallel to the input antenna 1 (see Fig. 2, *b*). The vertical dotted lines show the positions of the spectrum boundaries for longitudinally ($f_0^{\parallel}$) and transversely ($f_0^{\perp}$) magnetized waveguide calculated by formula (13), as well as the frequency $f_1^{\parallel}$ of the first width mode in this waveguide

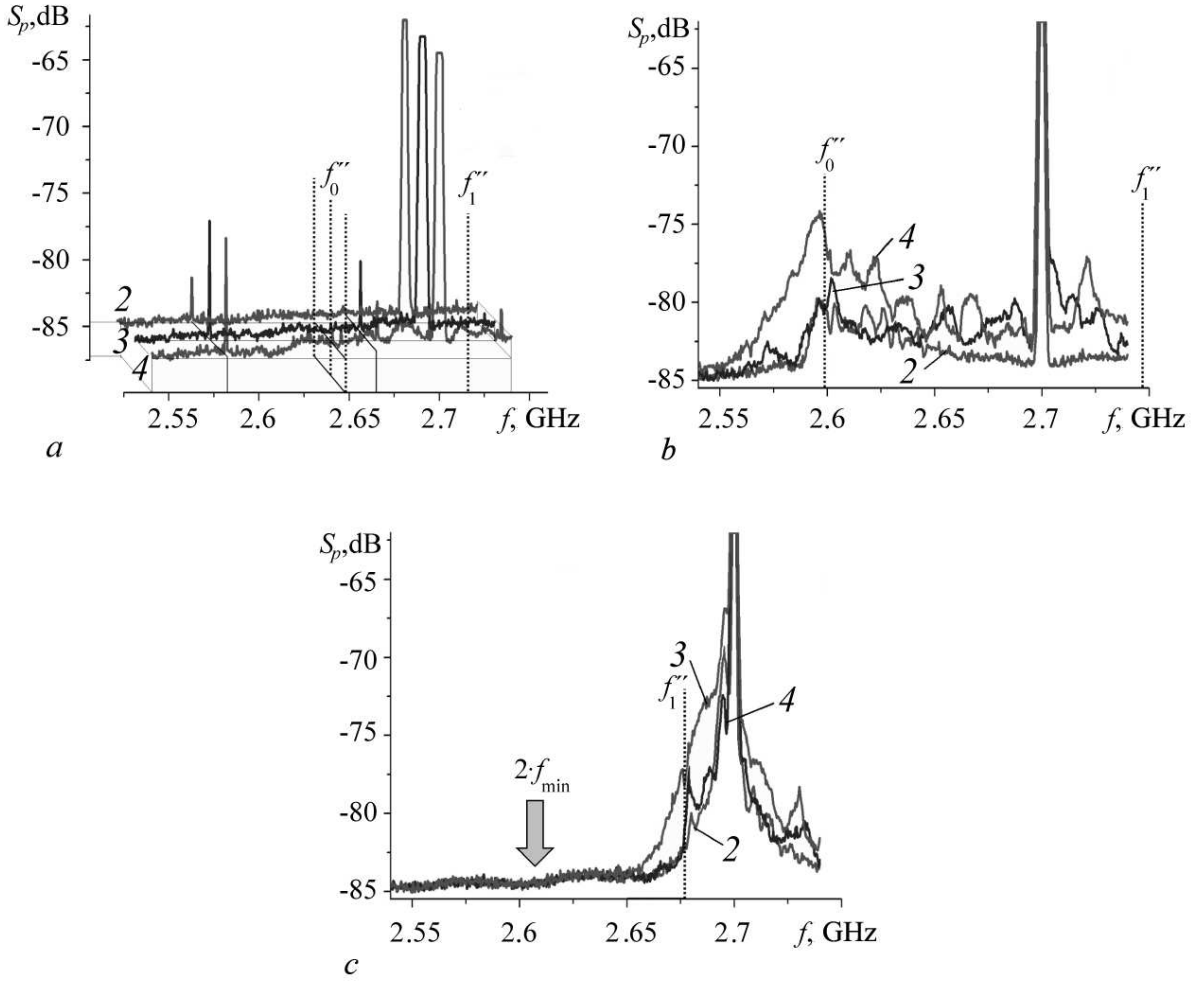

Fig. 6. The signal spectrum at the output antennas 2, 3 and 4, at the pump frequency of 2.7 GHz, magnetic field value of: *a* – 390 Oe, *b* – 415 Oe, *c* – 435 Oe. The digits near the curves correspond to the antenna number. The magnetic field $\vec{H}$ is perpendicular to the input antenna 1 (see Fig. 2, *b*). Above-critical value of pumping is $\approx 31...37$ dB. The dotted lines indicate the positions of the frequencies of uniform ferromagnetic resonance in the longitudinally ($f_0^{\parallel}$) and transversely ($f_0^{\perp}$) magnetized waveguide that is 3 mm long, 0.5 mm wide, 4 μm thick. Frequency $f_1^{\parallel}$ is the first width mode in this waveguide. The arrow in the fragment *c* shows the position of the frequency $2f_{min} \approx 2.61$ GHz

where n is an integer, and corresponds to the number of SW half-waves that fit along the width of the waveguides.

In the case shown in Fig. 2a, input transducer 1 can excite the SSW width mode of number n, which in the limit $k_{\|} \to 0$ has a "cutoff" frequency that coincides with the BVSW frequency and propagates along the magnetic field $\vec{H}$ with the wave number defined by expression (8). When the magnetic field $\vec{H}$ is oriented along the axis of the waveguide, the input antenna 1 will excite the width BVSW modes, for which the cutoff frequency for mode number n will coincide with the SSW frequency running perpendicular to the field with the wave number (8). With this in mind, in the long-wavelength approximation ($kd \ll 1$), the position of the cutoff frequencies in the spectrum of waveguides can be estimated using the relations

$$f_n^{\perp} \approx f_0^{\perp} - V_g^{\|} \frac{n}{2w}, \tag{9}$$

$$f_n^{\|} \approx f_0^{\|} + V_g^{\perp} \frac{n}{2w}, \tag{10}$$

where $V_g^{\|,\perp}$ are the group velocities of SSW and BVSW in infinite films for which in the long-wave approximation, one can obtain an estimate using the relations [38]

$$V_g^{\perp} = \frac{2\pi f_m d}{4} \frac{f_m}{f_0}, \tag{11}$$

$$V_g^{\|} = \frac{2\pi f_m d}{4} \frac{f_0}{f_m}. \tag{12}$$

It can be seen from (9) and (10) that for the width modes, the region of overlap of the SSW and BVSW spectra expands, and for the case when modes with $n = 1$ are excited in the waveguides, the region of overlap of the SSW and BVSW spectra is

$$\Delta f_1^{\|,\perp} = f_1^{\|} - f_1^{\perp} = \Delta f_0^{\|,\perp} + \frac{V_g^{\|} + V_g^{\perp}}{2w}. \tag{13}$$

For the selected structural parameters for modes with $n = 1$, the overlap region $f_1^{\|,\perp} \approx$ ≈ 0.3 GHz. If we compare the width of the "working" frequency bands $\Delta\Omega^{\|,\perp}$ defined according to the measurement results, in Fig. 3 with an estimate of the intervals $\Delta f_1^{\|,\perp}$ and $\Delta f_0^{\|,\perp}$, then we can see that $\Delta f_0^{\|,\perp} \le \Delta\Omega^{\|,\perp} \le \Delta f_1^{\|,\perp}$. This suggests that the experimentally recorded the signal filtering range in the cross-shaped structure under consideration is mainly determined by the overlapping region of the SW spectra $\Delta f_0^{\|,\perp}$ of mutually orthogonal waveguides forming a cross.

We now consider the spectra of the output signals in Fig. 4-6. Results shown in Fig. 4 and 5 correspond to the "SSW geometry" when the external field is directed along the antenna 1, which is optimal for excitation of the SSW. Fig. 6 shows the spectra for the "BVSW geometry", when the orientation of the external field is typical for the excitation of the BVSW. Here, the position of the "working" band $\Delta\Omega$ relative to the pump frequency f_p is taken into account. For clarity, in Fig. 4–6, the positions of the frequencies $f_{0,1}^{\|}$ and $f_0^{\perp}$ are marked by dashed line segments.

2.1. "SSW geometry". The spectra shown in Fig. 4 and 5 correspond to the case when antenna 1 excites SSW at a frequency $f_{p1} \approx 3$ GHz. The spectra in Fig. 4 correspond to pumping with a above-critical value $C \approx 21...29$ dB. Fig. 5 shows the results for $C \approx 31...38$ dB.

Note that the spectra of the signal from the output transducer 2 have a typical form for the selected ranges of above-critical values of pumping [27–31]. The appearance of satellines with the frequencies $F_s \neq f_p$ in the spectrum of SSW signal (see Fig. 4) is associated with thresholdless fusion of parametric spin waves with each other, which causes the appearance of secondary SSW, according to conservation laws [28]

$$f_1 + f_2 = F_s, \tag{14}$$

$$\vec{k}_1 + \vec{k}_2 = \vec{k}_s, \tag{15}$$

where the frequency F_s and the wave vector $\vec{k}_s$ of the secondary SSW correspond to some eigenmode (wave) of the structure, which is able to "reach" and be received by the output antenna. Note that the occurrence of secondary SSWs in the spectrum of intrinsic excitations of the structure ensures the resonant accumulation of the signal and allows it to be distinguished above the thermal noise level of the system. The fact that the condition $F_s \neq f_p$ turns out to be fulfilled in this case should be related to the fact that parametric spin waves with frequencies $f_1 \neq f_2$ participate in processes (14) and (15), and one of them has the frequency $f_1 = f_p/2$, and the other $f_2 = F_s - f_p/2$ [31]. The aforesaid is illustrated in Fig. 7, where the region of the phase space of the spectrum of spin waves is shown, which is populated by the parametric spin waves generated as a result of the decay processes (1), (2). The sections of the dispersion curves highlighted by circles and asterisks can satisfy the condition for the formation of satellites with frequencies $F_s \neq f_p$.

The appearance of the noise spectrum at high above-critical values (see Fig. 5) is associated with instability of parametric SW in the system [26]. In this case, the noise signal is characterized by a maximum near the frequency $2f_{min}$, which is tuned linearly by the magnetic field H.

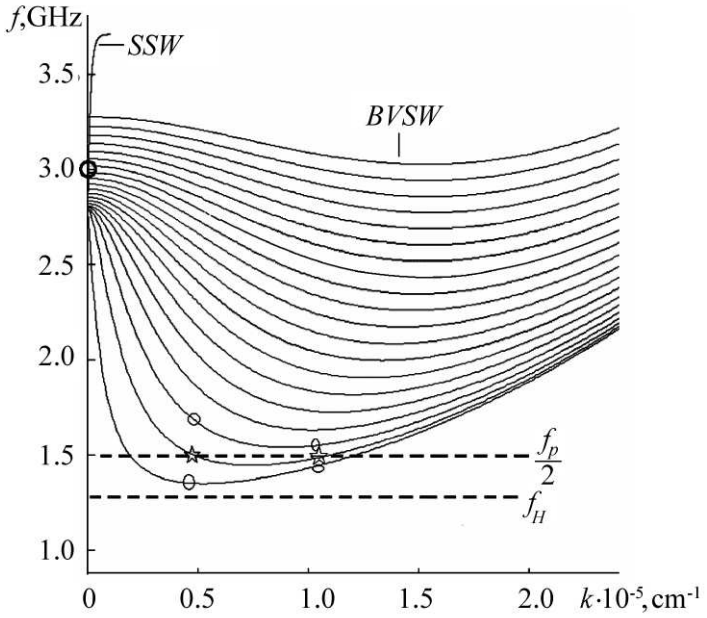

Fig. 7. The spectra of the SSW and BVSW modes with the numbers $m = 1, ..., 20$, calculated similar to [31], in the continuous film with the parameters corresponding to the studied YIG film placed in the field $H = 450$ Oe. The circle on the frequency axis indicates the position of the pump frequency $f_p \approx 3$ GHz. The horizontal dashed lines indicate the position of the frequencies f_H and $f_p/2$. Asterisks and circles in the spectrum indicate the regions producing parametric spin waves merging of which can lead to the formation of satellites with frequencies $F_s \neq f_p$

Let us compare the output spectra of signals from the antenna 2 with the spectra from the antennas 3 and 4 (Fig. 4). It can be seen that the spectra can differ markedly, and the degree of difference is determined by the position of the pump frequency f_p relative to the "working filtering band" $\Delta\Omega^{\perp}$. In this case, the farther the filtering band $\Delta\Omega^{\perp}$ from the pump frequency f_p, the smaller the number of satellites and their amplitude in the spectrum of output signals from antennas 3 and 4. This behavior is consistent with the presence of filtering properties of the cross-shaped structure. The mechanism of formation of secondary SWs (14), (15) should also be taken into account. Indeed, if the momentum conservation law (15) is fulfilled, the direction of the wave vector $\vec{k}_s$ can noticeably differ from the direction of the wave vector of the pump wave $\vec{k}_p$ [39]. Moreover, such waves can be received by an output transducer oriented orthogonally to the input. We note that the presence of $\vec{k}_s$ components perpendicular to the waveguide axis can lead to an increase in the satellite amplitude when its parameters $(F_s, \vec{k}_s)$ correspond to the lateral mode of the structure.

The presence of filtering properties in the cross-shaped structure is most noticeable in the case of high above-critical values of the pump signal when a noise spectrum is generated in the spectrum (see Fig. 5). It can be seen that the frequency band $\Delta\Omega^{\perp} \approx \Delta f_0^{\parallel,\perp}$ determines the width of the noise spectrum from the output of the antenna 3. It is also interesting to note that on the output antenna 2, the relative noise intensity in the spectrum of the output signal in the band $\Delta\Omega^{\perp} \approx \Delta f_0^{\parallel,\perp}$ is lower than in the spectrum of the signal at antenna 3. This should be related to the nature of the lateral modes of the transversely magnetized waveguide on which antenna 1 is located. Indeed, the bandwidth $\Delta f_0^{\parallel,\perp}$ is determined by the frequency shifts of $f_0^{\parallel}$ and $f_0^{\perp}$ relative to the frequency f_0. Using expressions (5) and (6), it is easy to show that it is the shift $\Delta f_0^{\perp}$ that is the main in the case under consideration. Remind that the frequency range $\Delta f_0^{\parallel,\perp}$ also corresponds to the SSW width modes having component of wave vector $k_{\perp}$ in the direction of the field defined by formula (8). In the case when, as a result of thresholdless fusion of parametric spin waves (14), (15), the wave vector $\vec{k}_s$ will have a projection onto the field direction close to $k_{\perp}$, the secondary SW will have the character of a width BVSW. Moreover, due to the proximity of F_s to the long-wavelength boundary $f_0^{\perp}$, the condition $k_{\perp} > k_{\parallel}$ can be fulfilled, and the secondary SW will correspond to the BVSW, "running" along the waveguide width. The orientation of its wavefront better corresponds to the effective reception of such a wave by transducers 3 and 4 than antenna 2. The proposed explanation is partly confirmed by the higher relative noise intensity at antenna 2 in the frequency range $[f_0^{\parallel}, f_p]$ in Fig. 5. Indeed, in the waveguide on which the antenna 1[1] is located, in the interval of frequencies $f > f_0^{\parallel}$, the resulting secondary SWs will have a longitudinal component of the wave number $k_{\parallel} \geq (2\pi\Delta f_0^{\perp})/V_g^{\perp} \approx 130\ \mathrm{cm}^{-1}$. In this case, for secondary satellite waves at frequencies F_s corresponding to "width" modes with $n \leq 5$, characterized in the case under consideration by values $k_{\perp} \leq 300\ \mathrm{cm}^{-1}$, the direction of the vector $\vec{k}_s$ will be within the SSW cutoff angle [24,25] , and thereby a greater correspondence between the secondary SW and SSW at the frequency F_s will be achieved.

However, the proposed signal filtering mechanism does not explain the significant difference in Fig. 5 in the spectra of signals at antennas 3 and 4, which in Fig. 4 was not so noticeable. In order to find out the possible connection of the indicated differences in the spectra from outputs 3 and 4 with the design features of the sample[2] (see Fig. 1), as well as with the heterogeneity and disorientation of field $\vec{H}$ with respect to the structure plane, experiments were carried out when antennas from 1 to 4 alternately acted as an input transducer. Qualitatively, the picture remained the same.

In order to show that the cross-shaped waveguide structure under consideration at high above-critical values of pumping can demonstrate different spectra of the output signals, micromagnetic

[1] Secondary SW are formed as the result of thresholdless processes of fusion (14), (15) that happen just close to the antenna 1.

[2] Position with respect to the ends of cross structure, orientation and parameters of antennas 1–4 differ, see Fig. 1.

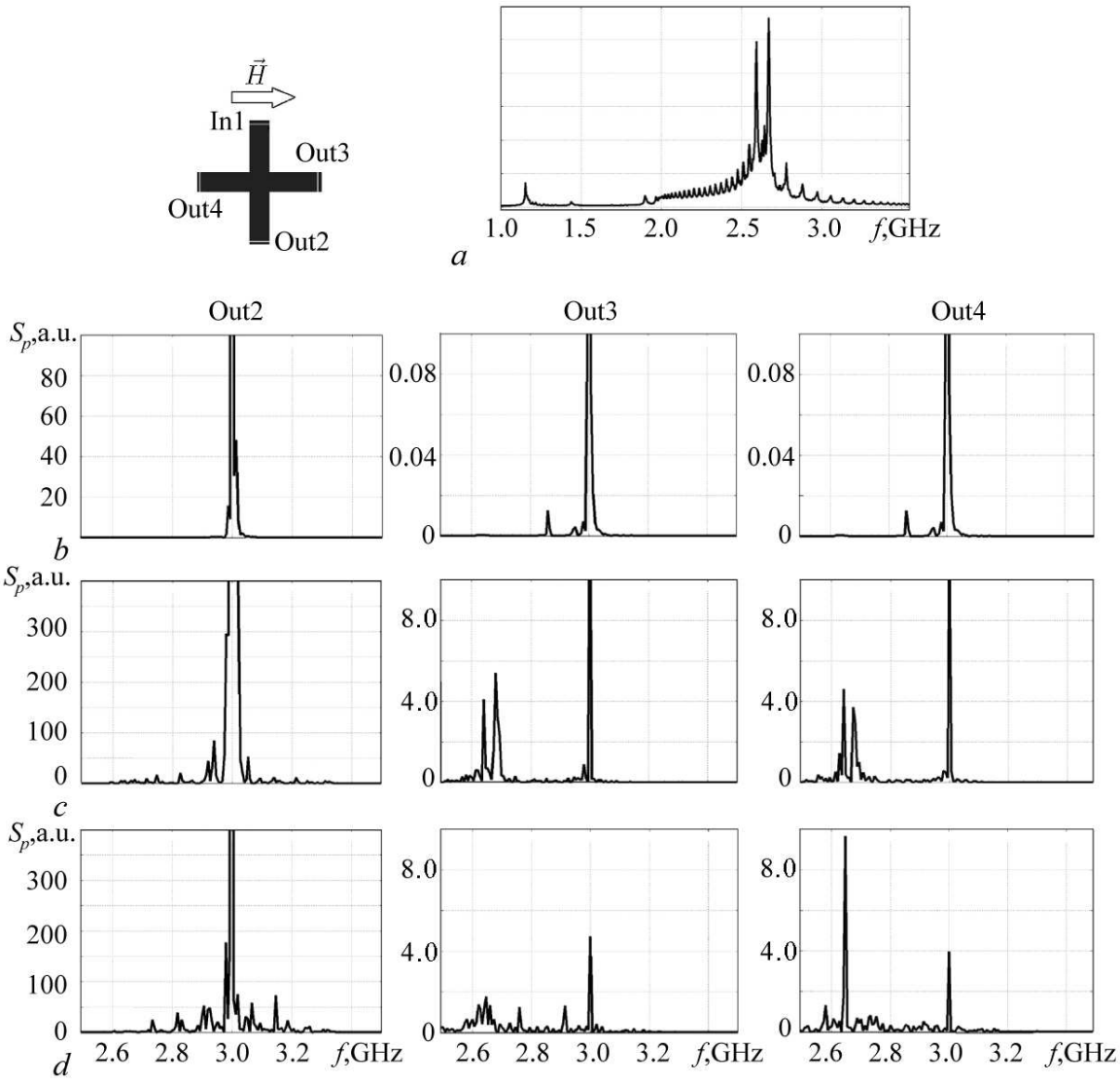

Fig. 8. Results of micromagnetic simulation having parameters analogous to experimental one. *a* – linear natural spectrum of the structure at field $H = 410$ Oe calculated in analogy with the method described in [37]. Field $\vec{H}$ is assumed to be directed along the input transducer 1 like it is shown in Fig. 2, *a*. Calculation of output signal spectra was carried out according to the method described in [37] for the different values of the amplitude of exciting field h_z, Oe at the input transducer 1: *b* – 20, *c* – 30, *d* – 50

simulation of the propagation of SWs in the structure under consideration was carried out within the framework of the approach described in [40]. Fig. 8 shows the results of micromagnetic modeling of the spectra of the output signals from antennas 2, 3, 4 with the field orientation $H = 410$ Oe, corresponding to the geometry of the experiment (see Fig. 2, *a*). In calculations, the antennas were assumed to be the same and had the same location relative to the ends of the cross. It can be seen that at high above-critical values, the spectra of the output signals on antennas 3 and 4 have qualitative differences. This, in our opinion, confirms the presence of mechanisms that can explain the difference in the spectra of the signals (shown in Fig. 4, 5) from the outputs 3 and 4 of the cross-shaped structure.

2.2. "BVSW geometry". The difference between this experiment geometry and the SSW case is a significant depletion of the spectra of the output signals. Moreover, due to the wider filtering

band $\Delta\Omega^{\parallel} \approx 0.3$ GHz, its effect on the shape of the spectrum is much less pronounced. However, this geometry is notable for the fact that here it is possible to observe the decay processes of width modes of the BVSW of the cross excited at frequencies $f_p > f_0^{\parallel}$ (see Fig. 6, *a*). At the field $H = 390$ Oe in a longitudinally magnetized waveguide with parameters corresponding to the cross-like structure, the frequency is $f_0^{\parallel} \approx 0.268$ GHz. In this case, the pump frequency $f_p \approx 2.7$ GHz is in the SSW frequency range occupied in the case of longitudinally magnetized waveguides with "width" BVSW modes. The satellites in the spectrum of the output signals in this case are secondary spin waves formed by the fusion of parametric spin waves into the SSW width modes, with frequencies $F_s \approx 2.66$ GHz, which corresponds to estimates of the cutoff frequency of the first BVSW width mode defined by expression (10). Satellites with frequencies $F_s \approx 2.58...2.6$ GHz fall into the frequency range $\Delta f_0^{\parallel,\perp}$ and can correspond to secondary BVSW.

Another feature of the considered geometry, in comparison with the geometry of SSW, is in reducing the number and amplitude of satellites in the spectrum of the output signal from antenna 2 relative to the case of antennas 3 and 4 (see Fig. 6, *a*, *b*). This is partly due to the fact that the orientation of the antenna 2 is not suitable for receiving the BVSW width modes at frequencies $f > f_0^{\parallel}$. Another circumstance that can affect the signal amplitude is the inhomogeneity of the ground state of the equilibrium magnetization of the cross-shaped structure, which, for the considered case of field $\vec{H}$ orientation leads to a decrease in the internal effective magnetic field in the center of the cross. In this case, for the BVSW with frequencies $f \approx f_0^{\parallel}$, the center of the structure will be perceived as a below cutoff section of the waveguide. It is possible that a low level of signal $S_{21}(f)$ is also associated with this, as compared with the level of $S_{31}(f)$ and $S_{41}(f)$ signals (see Fig. 3, *c*, *d*).

From Fig. 6, *b*, *c*, one can see that, with an increase in the field, accompanied by the approach of the pump frequency f_p to the doubled frequency of the "bottom" of the spectrum $2f_{min}$, the satellites broaden and form a noise-like pedestal near the pump frequency. For fields $H > 440$, for the selected pump frequency, condition (3) ceases to be satisfied, and three-magnon decay processes are forbidden by conservation laws (1), (2).

Conclusion

The effect of the first-order parametric processes on the propagation of spin waves in a tangentially magnetized cross-shaped structure based on a film of yttrium iron garnet has been experimentally studied.

- It is shown that due to the presence of filtering properties in structures based on orthogonal waveguides, the spectra of output signals under the conditions of the development of parametric instability are substantially determined by the position of the cross pass band in the frequency band of the analyzed spectrum.
- For the investigated structure from a film of yttrium iron garnet with a thickness $d \approx 3.8$ μm in the form of two orthogonal waveguides with a width of $w \approx 500$ μm and a length $L \approx 3$ mm, a significant influence of lateral quantization effects in the structure on the shape of the spectrum was established.
- For the first time, the processes of parametric decay of width modes of a longitudinally magnetized waveguide were investigated.
- It is also shown that with high above-critical values of pumping the types of signal spectra at the output antennas of orthogonally located cross-shaped waveguides can significantly differ.

References

1. Bernstein K., Cavin R. K., Porod W., Seabaugh A., Welser J. Device and architecture outlook for beyond CMOS switches. *Proc. IEEE.,* 2010, vol. 98, no. 12, pp. 2169–2184 .
2. Nikonov D.E., Young I.A. Overview of beyond-CMOS devices and a uniform methodology for their benchmarking. *Proc. IEEE,* 2013, vol. 101, no. 12, pp. 2498–2533.
3. Roy K., Bandyopadhyay S., Atulasimha J. Hybrid spintronics and straintronics: A magnetic technology for ultra low energy computing and signal processing. *Appl. Phys. Lett.,* 2011, vol. 99, 063108.
4. Chumak A.V., Vasyuchka V.K., Serga A.A., Hillebrands B. Magnon spintronics. *Nature Physics,* 2015, vol. 11, p. 453. DOI:10.138.NPHYS3347.
5. Nikitov S.A., Kaliabin D.V., Lisenkov I.V., Slavin A.N., Barabanenkov Yu.N., Osokin S.A., Sadovvnikov A.V., Baginin E.N., Morozova M.A., Sharaevskii Yu.P., Filimonov Y.A., Khivintsev Y.V., Vysotskii S.L., Sakharov V. K., Pavlov E.S. Magnonics: A new research area in spintronics and spin wave electronics. *Phys. Usp.,* 2015, vol. 58, no. 10, pp. 1002–1028. DOI: https://doi.org/10.3367/ UFNr.0185.201510m.1099
6. Khitun A., Wang K. Non-volatile magnonic logic engineering. *Journ. Appl. Phys.,* 2011, vol. 110, 0343061.
7. Khitun A. Magnonic holographic devices for special type data processing. *Journ. Appl. Phys.,* 2013, vol.113, 164503.
8. Nanayakkara K., Jacob A.P., Kozhanov A. Spin wave scattering and interference in ferromagnetic cross. *Journ. of Appl. Phys.,* 2015, vol. 118, 163904. DOI:10.1063/1.4934519.
9. Khitun A.G., Kozhanov A.E. Magnonic logic devices. *Izv. Sarat. University. New Serie Phisycs,* 2017. vol.17, no. 4, pp. 216–241.
10. Nanayakkara K., Anferov A., Jacob A. P., Allen S. J., Kozhanov A. Cross junction spin wave logic architecture. *IEEE Trans. on Magn.,* 2014, vol. 50, no. 11, 3402204.
11. Balynsky M., Kozhevnikov A., Khivintsev Y., Bhowmick T., Gutierrez D., Chiang H., Dudko G., Filimonov Y., Liu G., Jiang C., Balandin A.A., Lake R., Khitun A. Magnonic interferometric switch for multi-valued logic circuits. *Journ. of Appl. Phys.,* 2017, vol. 121, 024504.
12. Kozhevnikov A., Gertz F., Dudko G., Filimonov Y., Khitun A. Pattern recognition with magnonic holographic memory device. *Appl. Phys. Lett.,* 2015, vol. 106, no. 14, 142409.
13. Au Y., Davison T., Ahmad E., Keatley P.S., Hicken R.J., Kruglyak V.V. Excitation of propagating spin waves with global uniform microwave fields. *Appl. Phys. Lett.,* 2011, vol. 98, 122506.
14. Bracher T., Pirro P., Westermann J., Sebastian T., Lagel B., Van de Wiele B., Vansteenkiste A., Hillebrands B. Generation of propagating backward volume spin waves by phase-sensitive mode conversion in two-dimensional microstructures. *Appl. Phys. Lett.,* 2013, vol. 102, 132411.
15. Davies C.S, Francis A., Sadovnikov A.V., Chertopalov S.V., Bryan M.T., Grishin S.V., Allwood D.A., Sharaevskii Yu.P., Nikitov S.A., Kruglyak V.V. Towards graded-index magnonics: Steering spin waves in magnonic networks. *Phys. Rev. B,* 2015, vol. 92, no. 2, 020408.
16. Sadovnikov A.V., Davies C.S., Grishin S.V., Kruglyak V.V., Romanenko D.V., Sharaevskii Yu.P., Nikitov S.A. Magnonic beam splitter: The building block of parallel magnonic circuitry. *Appl. Phys. Lett.,* 2015, vol. 106, no. 19, 192406.
17. Demidov V., Demokritov S.O., Birt D., O'Gorman B., Tsoi M., Li X. Radiation of spin waves from the open end of a microscopic magnetic-film waveguide. *Phys. Rev. B,* 2009, vol. 80, 014429.
18. Dudko G.M., Kozhevnikov A.V., Khivintsev Yu.V., Filimonov Yu.A., Khitun A.G., Nikitov

S.A. Micromagnetic simulation of propagation of spin waves in in-plane magnetized crosses based on ferrite microwaveguides of different width. *Journ. of Communications Technology and Electronics,* 2018, vol. 63, Iss. 10, pp. 1212–1216. https://doi.org/10.1134/S1064226918100091.

19. Gertz F., Kozhevnikov A.V., Filimonov Y.A., Nikonov D., Khitun A. Magnonic holographic memory: From proposal to device. *IEEE Journ. on Exploratory Solid-State Computational Devices and Circuits,* 2015, vol. 1, pp. 67–75.
20. Balynskiy M., Chiang H., Gutierrez D., Kozhevnikov A., Filimonov Y., Khitun A. Reversible magnetic logic gates based on spin wave interference. *Journ. of Appl. Phys.,* 2018, vol. 123, 144501. DOI: 10.1063/1.5011772.
21. Khivintsev Y., Ranjbar M., Gutierrez D., Chiang H., Kozhevnikov A., Filimonov Y., Khitun A. Prime factorization using magnonic holographic devices. *Journ. of Appl. Phys.,* 2016. vol. 120, 123901. DOI: 10.1063/1.4962740.
22. Balynsky M., Gutierrez D., Chiang H., Kozhevnikov A., Dudko G., Filimonov Y., Balandin A.A., Khitun A. A magnetometer based on a spin wave interferometer. *Scientific Reports,* 2017, vol. 7, 11539.
23. Gutierrez D., Chiang H., Bhowmick T., Volodchenkov A.D., Ranjbar M., Liu G., Jiang C., Warren C., Khivintsev Y., Filimonov Y., Garay J., Lake R., Balandin A.A., Khitun A. Magnonic holographic imaging of magnetic microstructures. *Journ. of Magnetism and Magnetic Materials,* 2017, vol. 428, pp. 348–356. DOI:10.1016/j.jmmm.2016.12.022.
24. Gurevich A.G., Melkov G.A. Magnetization Oscillations and Waves. CRC Press. Boca Raton, 1996, 464 p.
25. Vashkovskiy A.V., Stal'makhov V.S., Sharayevskiy YU.P. Magnitostaticheskiye Volny v Elektronike Sverkhvysokikh Chastot. Izdatel'stvo Saratovskogo Universiteta, 1993. 311 p. (in Russian).
26. L'vov V.S. Nelineynyye Spinovyye Volny. M.:Nauka, 1987. 270 p. (in Russian).
27. Mednikov A.M. Nelineynyye effekty pri rasprostranenii poverkhnostnykh spinovykh voln v plenkakh ZHIG.*FTT,* 1981, vol. 23, Iss. 1, pp. 242–245 (in Russian).
28. Temiryazev A.G. Mekhanizm preobrazovanija poverhnostnoj magnitostaticheskoj volny v uslovijah trehmagnonnogo raspada. *FTT,* 1987, vol. 29, Iss. 2, pp. 313–319 (in Russian).
29. Melkov G.A., Sholom S.V. Parametric excitation of spin waves by a surface magnetostatic wave. *Sov. Phys. JETP (AIP),* 1989, 69, no. 2, p. 403.
30. Kazakov G.T., Kozhevnikov A.V., Filimonov Yu.A. Four-magnon decay of magnetostatic surface waves in yttrium iron garnet films. *Physics of the Solid State (Springer)*, 1997, vol. 39, Iss. 2, pp. 288–295.
31. Kazakov G.T., Kozhevnikov A.V., Filimonov Yu.A. The effect of parametrically excited spin waves on the dispersion and damping of magnetostatic surface waves in ferrite films. *Journ. of Exper. and Theor. Phys.(AIP)*, 1999, vol. 88, no. 1, pp. 174–181. DOI:10.1134/1.558780.
32. O'Keeffe T.W., Patterson R.W. Magnetostatic surface-wave propagation in finite samples // *J. Appl. Ptys.,* 1978, vol. 49, pp. 4886–4895.
33. Sadovnikov A.V., Odintsov S.A, Beginin E.N., Grachev A.A., Gubanov V.A., Sheshukova S.E., Sharaevskii Yu. P., Nikitov S.A. Nonlinear spin wave effects in the system of lateral magnonic structures. *JETP Letters,* 2018, vol. 107, Iss. 1, pp. 25–29. DOI:10.1134/S0021364018010113.
34. Sadovnikov A.V., Odintsov S.A., Beginin E.N., Sheshukova S.E., Sharaevskii Yu.P., Nikitov S.A.

Toward nonlinear magnonics: Intensity-dependent spin-wave switching in insulating side-coupled magnetic stripes. *Phys. Rev. B*, 2017, vol. 96, 144428.

35. Sadovnikov A.V., Davies C.S., Kruglyak V.V., Romanenko D.V., Grishin S.V., Beginin E.N., Sharaevskii Y.P., Nikitov S.A. Spin wave propagation in a uniformly biased curved magnonic waveguide. *Phys. Rev. B,* 2017, vol. 96, 060401(R).
36. Polzikova N.I., Raevskii A.O., Temiryazev A.G. Vlilanie obmennogo vzaimodejstvija na granitsu trehmagnonnogo raspada volny Damona-Eshbacha v tonkih plenkah YIG. *FTT,* 1984, vol. 26, iss. 11, pp. 3506–3508 (in Russian).
37. magpar – Parallel Finite Element Micromagnetics Package Version 0.9 Build 3061M (2002). www.magpar.net/static/magpar/doc/html/index.html
38. Stancil D.D., Prabhakar A. Spin Waves: Theory and Applications. Springer Science+Business Media, *LLC,* 2009, no. 2008936559. DOI 10.1007/978-0-387-77865-5.
39. Grechushkin K.V., Stalmakhov A.V., Tyulyukin V.A. Prostranstvennaja structura puchkov voln-satellitov nelinejnoi poverhnostnoj magnitostaticheskoj volny. *Radiotechnika i Electronica,* 1991, vol. 36, pp. 2078–2084 (in Russian).
40. Dudko G.M., Khivintsev Y.V., Sakharov V.K., Kozhevnikov A.V., Vysotskii S.L., Seleznev M.E., Filimonov Y.A., Khitun A.G. Micromagnetic modeling of nonlinear interaction of lateral magnetostatic modes in cross-shaped structures based on waveguides from iron yttrium garnet films. *Izvestiya VUZ. Applied Nonlinear Dynamics,* 2019, vol. 27, no. 2, pp. 39–60 (in Russian). DOI:https://doi.org/10.18500/0869-6632-2019-27-2-39-60.